J. Fluid Mech. (1976), *vol.* 75, *part* 1, *pp.* 49–79
Printed in Great Britain

Axisymmetric convection in a rotating sphere. Part 1. Stress-free surface

By A. D. WEIR

Department of Aeronautics, Imperial College, London

(Received 5 February 1975 and in revised form 6 August 1975)

This paper examines large-scale nonlinear thermal convection in a rotating self-gravitating sphere of Boussinesq fluid containing a uniform distribution of heat sources. Conservative finite-difference forms of the equations of axisymmetric laminar motion are marched forward in time. The surface is assumed to be stress free and at constant temperature. Numerical solutions are obtained for Taylor numbers in the range $0 \leqslant \Lambda \leqslant 10^4$ and Rayleigh numbers with

$$R_c \leqslant R \lesssim 10R_c.$$

For high Prandtl number ($P > 5$) the solutions are steady and most of them resemble the solutions of the linear stability equations, though other steady solutions are also found. For $P \lesssim 1$, the steady solutions have horizontal wavenumber $l = 1$ and nearly uniform angular momentum per unit mass, rather than nearly uniform angular velocity. This rotation law seems to be independent of many details of the model and may hold in the convective core of a rotating star.

1. Introduction and summary

The structures of many stars and planets are known to be greatly influenced by thermal convection in their interiors and by rotation of the body as a whole, but though the separate effects of these processes have been fairly well studied, their interaction, especially for well-developed flows in a sphere, has not. This paper examines the combined effect of bulk rotation, nonlinearity and spherical geometry on a convecting system, and will show by numerical integration of the (axisymmetric) equations of motion that the interaction of these effects can produce behaviour which would not be predicted by considering them in isolation.

In particular, under certain conditions, the meridional motions can be sufficiently strong to redistribute the angular momentum of the system, resulting in a steady state like that shown in figure 7, in which the angular momentum per unit mass is nearly uniform over the convecting region. The detailed fluid dynamics of this particular situation are discussed in §6, and its application to models of rotating stars in §7, where it is suggested that this result may resolve a degeneracy in the theory of such stars which has so far hindered comparisons with observation, by fixing the relation of the observable velocity at the surface to the unobservable angular velocity of the interior.

The model system considered in this paper is just complicated enough to

show all the influences mentioned above, but sufficiently simple that its exact equations of motion can be solved numerically on present-day computers. The model consists of a uniformly heated self-gravitating sphere of Boussinesq fluid. The temperature at the surface is held constant, and the surface itself is taken as stress free, a reasonable first approximation for the convective core of a massive star. A later paper will describe the case of a rigid (no-slip) surface, a better model for the fluid core of a planet.

In order to treat a wide range of flow parameters without exorbitant use of computer resources, only axisymmetric flows are considered. Though stability theory for this model (Roberts 1968; Busse 1970*a*) suggests that such flows are unlikely to occur at very high rotation rates, they can still reveal many of the effects of nonlinearity, bulk rotation and spherical geometry, and are therefore of intrinsic fluid dynamic interest.

This paper exhibits three ways in which an axisymmetric motion can overcome the restraining effect of rotation expressed by the Taylor–Proudman theorem: namely by viscous transfer of angular momentum (§5), by close packing of cells (§5) and by nonlinear advection of angular momentum (§6). These mechanisms are all relevant in the non-axisymmetric case, though they may take a different form. In the absence of rotation (§4), the assumption of axisymmetry is not so restrictive, as shown by the linear theory of Chandrasekhar (1961, chap. 6), which is independent of the azimuthal wavenumber m, and by the numerical experiments of Young (1974), who found that axisymmetric solutions were often preferred, and even where they were not preferred, they still gave a fair guide to the gross behaviour of the system.

Though much previous work has shown that rotation inhibits the onset of convection in a variety of situations (Chandrasekhar 1961), the effect of rotation on a strongly nonlinear convective flow has so far been studied only for the case of a plane layer heated from below. Most theoretical investigations of this case (e.g. Veronis 1968; Somerville & Lipps 1973) have used equations which fail to specify the precise position in the system of the axis of rotation, thereby concealing the important physical distinction between angular momentum and angular velocity, and making it difficult to interpret the effect of the convective motions on the original rotation. This difficulty and the related one of choosing a horizontal wavenumber for the flow are automatically overcome by explicitly considering the spherical geometry appropriate to a stellar core. This also introduces another effect which may be important, namely that the angle between the buoyancy forces and the rotation forces varies with latitude, so that motions near the poles differ qualitatively from those near the equator even if the heating is uniform.

A clearer feedback of convection to the underlying rotation, in the form of an equatorial acceleration at the surface, was found by Busse (1970*b*, 1973) and Durney (1970) in their studies of mildly nonlinear convection in a slowly rotating spherical shell. They found that the preferred mode had $m \sim \eta$, the ratio of the inner to the outer radius of the shell. In the present case $\eta = 0$, so that axisymmetric motions ($m = 0$) may be more relevant here than in a shell.

The precise formulation of the model and its equations of motion is given in

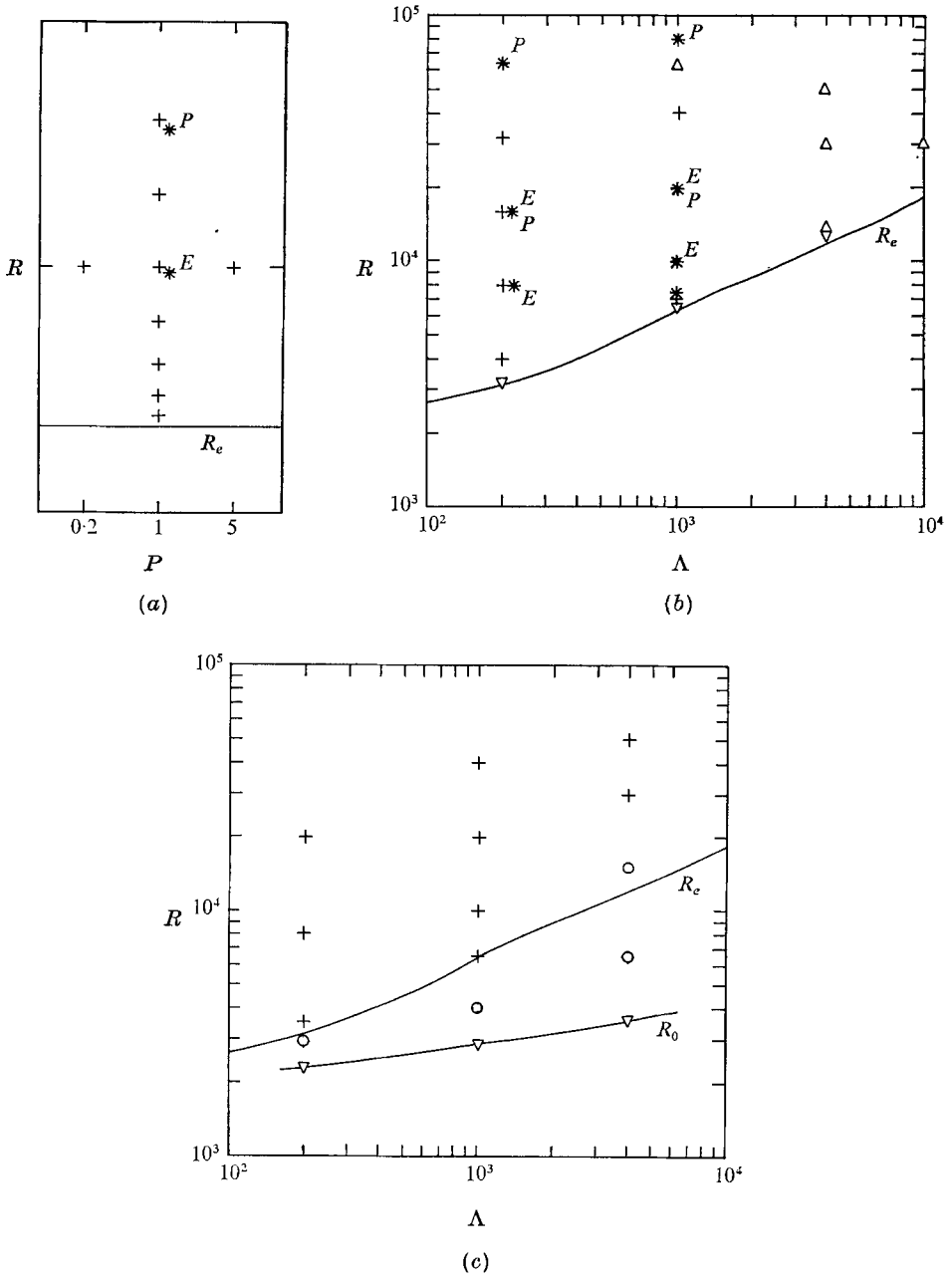

FIGURE 1. Cases computed with (*a*) $\Lambda = 0$, (*b*) $P = 5$, $\Lambda > 0$ and (*c*) $P = 0{\cdot}2$, $\Lambda > 0$. Symbols indicate the type(s) of sustained flow found at each Prandtl number P, Taylor number Λ and Rayleigh number R; +, steady single cell; *, steady double cell (E = falling at equator, P = falling at poles); △, steady triple cell; ○, sustained (single-cell) oscillation. Curve R_e is the 'exchange of stabilities' according to Roberts (1968); curve R_0 is the onset of overstability, as found here. Note the existence of several solutions at one (Λ, R) with $P = 5$, and of oscillatory solutions with $P = 0{\cdot}2$, but not the converse.

§2, and the finite-difference schemes used to solve the equations are described in §3. The flow is determined by the initial conditions and three dimensionless parameters defined in §2: the Prandtl number P, Taylor number Λ and Rayleigh number R. The numerical scheme is effective for only a limited range of (P, Λ, R), namely $0{\cdot}1 \lesssim P \lesssim 10$, $0 \leqslant \Lambda \lesssim 10^4$, $0 \leqslant R \lesssim 10^5$, but this is sufficient to exhibit the three major regimes of 'two-dimensional' convection. In accordance with earlier theoretical (Chandrasekhar 1961; Veronis 1968) and experimental work (Rossby 1969) on a plane layer heated from below, the parameter space divides into three distinct regions: (*a*) $\Lambda = 0$, (*b*) $\Lambda > 0$, P large and (*c*) $\Lambda > 0$, P small, the results for which are described in §§4, 5 and 6 respectively. Figure 1, which shows the form of the solution(s) found at each (P, Λ, R) studied, illustrates the differences between the regimes.

The flows with $\Lambda = 0$ (figure 1*a*) allow simple physical interpretation, uncluttered by the effects of bulk rotation. Though a single-cell solution is most common, some higher modes can be forced at sufficiently high Rayleigh numbers by taking suitable initial conditions. The two-cell mode shows an interesting distinction between the rising and falling plumes. Varying the Prandtl number between 0·1 and 10 has remarkably little effect on these flows, thus allowing a useful comparison with the similar computations of Hsui, Turcotte & Torrance (1972) with $P = \infty$ and $\Lambda = 0$.

The case of a rotating system with 'large' P is represented here by $P = 5$ (figure 1*b*). Nonlinear effects, such as advection of vorticity, are weak and most of the well-developed flows have the same form as the solutions of the marginal-stability equations, i.e. as Λ increases, the cells are compressed normal to the axis, with a corresponding rise in wavenumber. Though there is a weak tendency for the number of cells to increase with Rayleigh number, a range of solutions can again be obtained by varying the initial conditions.

With a 'small' Prandtl number (represented here by $P = 0{\cdot}2$; figure 1*c*), rotation allows convection to occur as oscillatory motions at Rayleigh numbers for which the static solution is stable at large P. Oscillations of remarkably large amplitude can be sustained and are described in §6. At higher Rayleigh numbers, nonlinear effects force the flow to be of the form in figure 7, with a single large convection cell maintaining a region of uniform angular momentum.

2. Mathematical formulation of the model

2.1. *Equations of motion*

The full equations of thermal convection in the Boussinesq approximation may be written in the form

$$\partial \mathbf{u}/\partial t + \mathbf{u}.\nabla\mathbf{u} + 2\boldsymbol{\Omega} \times \mathbf{u} = -(\nabla p)/\rho + \mathbf{g}\alpha(T - T_e) + \nu\nabla^2\mathbf{u}, \tag{1}$$

$$\partial T/\partial t = H - \operatorname{div}(\mathbf{u}T) + \kappa\nabla^2 T, \tag{2}$$

$$\operatorname{div}\mathbf{u} = 0, \tag{3}$$

in which $\mathbf{u}(\mathbf{x})$ is the fluid velocity, measured in a frame rotating with uniform angular velocity with respect to an inertial frame, p is a modified pressure, ρ

is the (nearly constant) density, $\mathbf{g}$ is the acceleration due to gravity, α is the coefficient of thermal expansion, $T(\mathbf{x})$ is the actual fluid temperature, $T_e(\mathbf{x})$ is that in static equilibrium, ν is the kinematic viscosity, κ is the thermal diffusivity, and $H' = H\rho c_p$ is the internal heating per unit volume per unit time, c_p being the specific heat.

For a uniform self-gravitating fluid sphere of radius r_0, the inward gravitational force per unit mass at a radius r from the centre is

$$\mathbf{g}(r) = -\tfrac{4}{3}\pi\rho G\mathbf{r} = -g(r)\,\hat{\mathbf{r}}, \tag{4}$$

where G is the gravitational constant and $\hat{\mathbf{r}}$ is a unit vector.

In conductive equilibrium, the temperature distribution is given by

$$T_e(r) = (H/6\kappa)\,(r_0^2 - r^2). \tag{5}$$

We may take (1)–(3) to be dimensionless by taking the units of length, time and temperature to be r_0, r_0^2/κ and Hr_0^2/κ respectively. This reveals that the system is characterized by only three independent dimensionless parameters; we take these to be the Prandtl number

$$P = \nu/\kappa, \tag{6}$$

the Taylor number
$$\Lambda = (2\Omega r_0^2/\nu)^2 \tag{7}$$

and the Rayleigh number

$$R = \left(\frac{3}{4\pi}\right)\left(\frac{Hr_0^2}{\kappa}\right)\frac{g(r_0)\,\alpha r_0^3}{\kappa\nu}. \tag{8}$$

We shall neglect the centrifugal force compared with true gravity; formally speaking, we take the limit

$$\alpha \to 0, \quad g(r_0) \to \infty, \quad \alpha g(r_0) = \text{constant}. \tag{9}$$

This also allows us to neglect distortion of the outer surface by rotation.

Throughout this paper, we shall use spherical polar co-ordinates (r, θ, ϕ) such that $\theta = 0$ is the axis of rotation. We shall refer to the point $(r = 1, \theta = 0)$ as the 'north pole'. We consider only axisymmetric motions, so that $\partial/\partial\phi = 0$. Then (3) allows us to define a (Stokes) stream function ψ such that at the position $\mathbf{r} = (r, \theta, \phi)$ the velocity is

$$\mathbf{u} = (w, u, v) = \left(\frac{1}{r^2 s}\frac{\partial\psi}{\partial\theta}, -\frac{1}{rs}\frac{\partial\psi}{\partial r}, v\right) \tag{10}$$

and the vorticity is

$$\boldsymbol{\omega} = \nabla\times\mathbf{u} = (\xi, \eta, \zeta) = \left(\frac{1}{rs}\frac{\partial(vs)}{\partial\theta}, -\frac{1}{r}\frac{\partial(vr)}{\partial r}, \zeta\right),$$

where $s = \sin\theta$.

We shall occasionally use cylindrical co-ordinates (ϖ, ϕ, z) in which

$$\varpi = rs, \quad z = r\cos\theta \tag{11}$$

are respectively displacements perpendicular to and parallel to the axis of rotation (which is the z axis), and ϕ is as before. The velocity at (ϖ, ϕ, z) will be denoted by (U, V, W).

We eliminate the pressure p by taking the curl of (1), which becomes (after using standard vector identities)

$$\partial\boldsymbol{\omega}/\partial t = \nabla\times(\mathbf{u}\times\boldsymbol{\omega}) + \nabla\times(\mathbf{u}\times 2\boldsymbol{\Omega}) + \nabla\times(g\alpha T\hat{\mathbf{r}}) - \nu\nabla\times(\nabla\times\boldsymbol{\omega}), \tag{12}$$

the ϕ component of which can be expanded as

$$\begin{aligned}\frac{\partial\zeta}{\partial t} = {} & \frac{1}{r}\frac{\partial}{\partial r}(rv\xi - rw\zeta) - \frac{1}{r}\frac{\partial}{\partial\theta}(u\zeta - v\eta) \\ & + \frac{2\Omega}{r}\left[\frac{\partial}{\partial r}(rv\cos\theta) - \frac{\partial}{\partial\theta}(v\sin\theta)\right] \\ & - \frac{g\alpha}{r}\frac{\partial T}{\partial\theta} + \frac{\nu}{r}\left[\frac{1}{r}\frac{\partial}{\partial\theta}\left(\frac{1}{s}\frac{\partial(\zeta s)}{\partial\theta}\right) + \frac{\partial^2}{\partial r^2}(\zeta r)\right].\end{aligned} \tag{13}$$

The ϕ component of (1), usually written as (Batchelor 1967, p. 601)

$$\begin{aligned}\frac{\partial v}{\partial t} + w\frac{\partial v}{\partial r} + \frac{u}{r}\frac{\partial v}{\partial\theta} + \left(2\Omega + \frac{v}{r\sin\theta}\right)(w\sin\theta + u\cos\theta) \\ = -\nu\hat{\boldsymbol{\phi}}.\operatorname{curl}\operatorname{curl}\mathbf{u},\end{aligned} \tag{14}$$

may be transformed by standard vector identities into a form more explicitly expressing the conservation of angular momentum $L = v\varpi + \Omega\varpi^2$, namely

$$\frac{\partial v}{\partial t} + \frac{1}{rs}\operatorname{div}(\mathbf{u}vrs) + \frac{\Omega}{rs}\operatorname{div}(\mathbf{u}r^2s^2) = \frac{\nu}{rs}[\operatorname{div}\operatorname{grad}(vrs) - 2\operatorname{div}(v\hat{\boldsymbol{\varpi}})], \tag{15}$$

where $\hat{\boldsymbol{\varpi}} = (\sin\theta, \cos\theta, 0)$ is a unit vector perpendicular to the axis. Similarly, (13) may be written in the form

$$\frac{\partial\zeta'}{\partial t} + \operatorname{div}(\mathbf{u}\zeta') = -\frac{g\alpha}{r^2 s}\frac{\partial T}{\partial\theta} + \ldots, \tag{16}$$

where $\zeta' = \zeta/rs$ corresponds to the circulation around a small fluid element.

Finally, it follows analytically from (10) that

$$\zeta = \hat{\boldsymbol{\phi}}.\operatorname{curl}\mathbf{u} = \frac{1}{rs}\left[-\frac{\partial^2\psi}{\partial r^2} - \frac{1}{r^2}\frac{\partial^2\psi}{\partial\theta^2} + \frac{\cot\theta}{r^2}\frac{\partial\psi}{\partial\theta}\right], \tag{17}$$

which must be satisfied in a consistent solution.

2.2. *Conditions at surface and axis*

For simplicity, we take the outer surface to be at constant temperature, and to be undistorted by rotation or rising plumes. Then, neglecting irrelevant additive constants, we have

$$T = \psi = 0 \quad \text{at} \quad r = r_0, \tag{18}$$

which, with (17), implies

$$\zeta = -(rs)^{-1}\,\partial^2\psi/\partial r^2 \quad \text{at} \quad r = r_0. \tag{19}$$

For an axisymmetric system, the condition of zero tangential stress (and therefore zero tangential shear) at the surface implies

$$\frac{\partial}{\partial r}\left(\frac{v}{r}\right) = \frac{\partial}{\partial r}\left(\frac{\partial\psi/\partial r}{r^2}\right) = 0 \quad \text{at} \quad r = r_0. \tag{20}$$

At the axis, the axisymmetry and the requirement that the angular velocity be finite imply

$$\psi = \zeta = v = 0 \quad \text{at} \quad r = 0 \quad \text{or} \quad s = 0. \tag{21}$$

3. Numerical method

3.1. *Choice of method*

All the results described below have been obtained by solving finite-difference analogues of (2), (13), (15) and (17), subject to the boundary conditions (18)–(20) and the axis conditions (21). These particular equations were chosen, in preference to other analytically equivalent forms, because even in their finite-difference forms, they express the conservation of matter, angular momentum and energy.

Difference methods are favoured in a spherical geometry as they combine reasonable accuracy with ease of implementation. Galerkin methods (Orszag & Israeli 1974) are most useful in a rectangular geometry, where the fast Fourier transform can be used to advantage, while finite-element methods (Brebbia & Connor 1974, p. 325) are better in more irregular geometries. The analyses of Moore, Peckover & Weiss (1973) and Morton (1971) suggest that, for problems like that considered here, conservative difference schemes of second-order accuracy are the simplest to give reasonable accuracy. Higher-order schemes do not yield an increase in overall accuracy proportionate to their greater complication, while non-conservative schemes give unacceptable distortion of the physics.

The numerical method used is therefore an extension to spherical geometry of the conservative second-order scheme of Moore *et al.* (1973). The details are given in an appendix, as they may be useful for other work on spherical flows, and so that readers may independently assess the scheme.

3.2. *Accuracy and stability*

In the present scheme both sides of the difference equation refer to the same point in space-time, and so time-dependent solutions can be followed accurately, which is an advantage when these are the physically interesting solutions, as in §6.3. Difference equations which do not have this property are both difficult to interpret physically and prone to numerical instabilities and inaccuracies (Morton 1971).

The divergence terms in (2) represent fluxes of energy (T) from neighbouring elements of fluid. As shown by Roberts & Weiss (1966), by deriving one's finite-difference equations as explicit representations of these fluxes, one ensures that the difference scheme merely redistributes the energy input by the sources H, as in the physical system – a desirable property not shared by many other numerical schemes. The difference form (A 4) of (15) would similarly merely redistribute angular momentum were it not for a subtle error in the boundary conditions, discussed below.

The truncation errors of all the formulae used in the interior are formally of second order, except for (A 11), which is of fourth order. However, though the

solution Φ_{jk} of the difference equations at (r_j, θ_k) differs by second-order terms from that of the differential equations, evaluated at the same point, the former has a different physical meaning, namely the average value over the elementary volume centred on (r_j, θ_k). Unfortunately, the same value is used in the difference equations as the average over one face of the volume centred on (r_{j+1}, θ_k), which introduces a different kind of second-order error (Roberts & Weiss 1966). The values of ψ, however, are meaningful as spot values.

The numerical boundary conditions (18) are exact, while (A 15) and (A 16) are formally accurate to second order. Despite appearances (A 17) is accurate only to $O(h)$, because the second derivative is evaluated from only two independent values of ψ, namely $\psi_{J-1,k}$ and $\psi_{J,k}$. The experience of Moore *et al.* (1973) was that boundary conditions accurate to order $n-1$ did not significantly impair the accuracy of a scheme accurate to order n in the interior, so the simple scheme (A 17) should give values of ζ that are adequately accurate, especially as no important conservation principle is associated with ζ.

The best way to estimate the effect of these truncation errors is not to evaluate the coefficients buried in the $O(h^2)$ symbolism, but rather to compare solutions obtained with meshes of different spacing (h, δ), both with each other and (where possible) with known analytic solutions. For example, the numerical solution on a 16×16 mesh of (A 1) with $\psi = 0$ yields a conductive temperature distribution differing by less than 0·01 % from the exact solution (5).

Most of the results described below were obtained with a 16×16 mesh, as the results of Moore & Weiss (1973) indicated that this would give adequate accuracy for flows with $R \lesssim 20R_c$. A few of the runs were repeated with a 48×48 mesh, and it was found that the numerical values of $\psi(r, \theta)$, $T(r, \theta)$ etc. obtained differed by less than 1 % from those obtained on the coarser mesh, which gives confidence in the solutions.

Comparison with independent 'accurate' values not of the field variables themselves, but of gross parameters like $R_c(\Lambda)$ gives a useful measure of the truncation errors. Indeed, this is how I estimated the range of (R, Λ, P) over which the computations were reliable.

The importance of using conservative schemes was illustrated by the results obtained when the conservative difference scheme (A 4) for $\Delta v/\Delta t$ was replaced by one based on the non-conservative equation (14). This gave a 20 % difference in the computed values of ψ and v, though the form of the solution did not change.

By using Gauss' theorem to integrate (15) over the whole sphere, it can be shown that the boundary condition (20) on the tangential stress ensures that no angular momentum passes through the surface of the sphere. Unfortunately, the numerical condition (A 15), though formally an accurate analogue of (20), does not quite share this property. In the computed flows, spurious angular momentum leaks through the boundary, though so slowly that consistent quasi-steady states can still be obtained in the range of (R, Λ, P) considered here, and it is these that are described below. It was found afterwards that this trouble arises from the treatment of the advection terms in (A 4) in the elementary volumes with $r_{J-1} \leqslant r \leqslant r_{J+1}$, which straddle the boundary. It would seem that,

for accurate results, it is insufficient merely to represent a flux boundary condition such as (20) to high formal accuracy while still applying one's usual scheme throughout the interior; special formulae must also be used for points near the boundary, and the staggered mesh modified to fit. The effect of this leak on particular computed flows is discussed in §§5 and 6.

The schemes are always stable provided that the time step satisfies the Courant–Friedrichs–Lewy conditions

$$w\Delta t/h < 1, \quad u\Delta t/r\delta < 1. \tag{22}$$

For the diffusion terms to be reasonably accurate, one also requires

$$\nu\Delta t/h^2 \lesssim 1, \quad \kappa\Delta t/h^2 \lesssim 1. \tag{23}$$

In normal running Δt is initially chosen to satisfy (23) and, at each time step, the program checks that (22) is satisfied. If not, then Δt is halved and computation continues.

The numerical scheme (including the solution of the elliptic equation (17)) is such that rounding errors are much less than truncation errors, even when using single-precision arithmetic on an IBM 370 (which works to only about 7 decimal places).

4. Results with zero rotation

For $P \gg 1$, the condition (23) on Δt become irksome, and for $P \ll 1$, momentum diffuses so slowly that a very long time elapses before a steady state is obtained. Therefore, most of the computations with zero rotation were made with Prandtl number $P = 1$. Later calculations (§4.3) showed that the qualitative effect of varying P was small when $\Lambda = 0$, thus allowing quantitative comparisons to be drawn with the earlier calculations of Hsui *et al.* (1972), who used a different numerical method to look at the same problem, but considered only the case $\Lambda = 0, P = \infty$.

A first check on the present program is to see that the numerical experiments agree with linear stability theory (Chandrasekhar 1961, p. 235) where the latter applies, namely to the growth of small disturbances from conductive equilibrium. The numerical experiments with $\Lambda = 0$ showed the predicted behaviour: instability set in as a direct (i.e. non-oscillatory) single-cell mode at

$$R_c = (2{\cdot}24 \pm 0{\cdot}03) \times 10^3$$

in excellent agreement with the value of 2214 given by linear stability theory.

4.1. *Single-cell flows with* $P = 1, \Lambda = 0$

No oscillatory flows were found with $P = 1, \Lambda = 0$; given enough time the flow always reached a steady state, to which it was usually close after one or two turnover times. In the units used here, the turnover time of a cell is $\tau_e \approx \psi_m^{-1}$, where ψ_m is the maximum value of the stream function. Figure 2(*a*) shows a typical steady flow, obtained from an initial weak single-cell disturbance to conductive equilibrium.

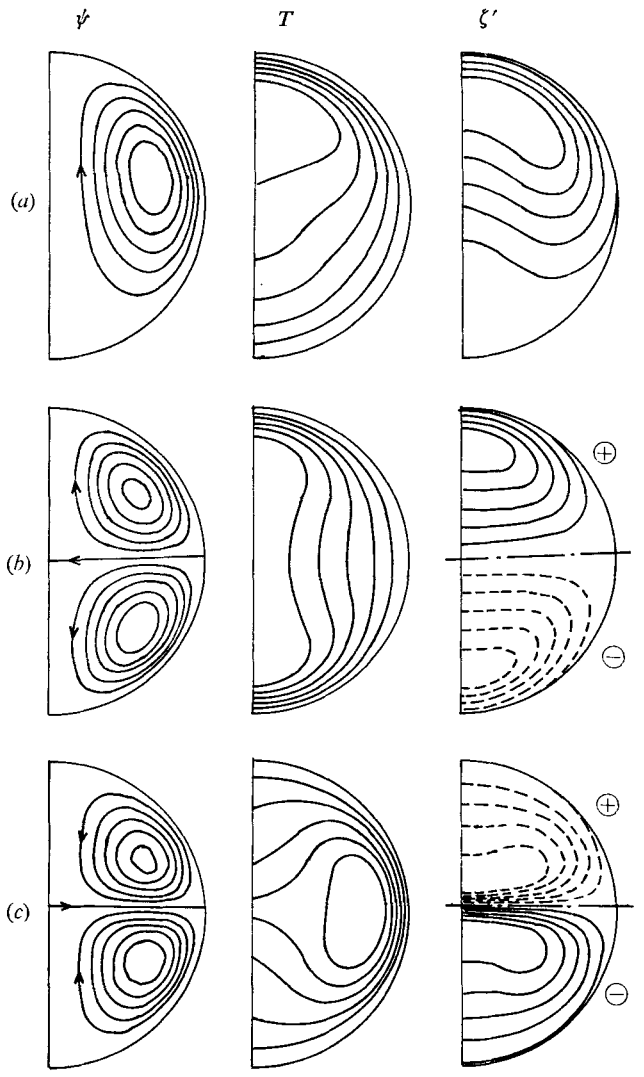

FIGURE 2. Contours of stream function ψ, temperature T and 'vorticity' ζ' for steady convection in a uniformly heated fluid sphere. Flows are symmetric about the vertical diameter. Arrows show direction of flow; dashed contours of ζ' show negative values. Prandtl number $P = 1$, Taylor number $\Lambda = 0$.

	R	max ψ	max T	max ζ'
(*a*)	10000	2·86	0·110	205
(*b*)	10000	1·56	0·112	296
(*c*)	40000	4·43	0·063	508

We note that the hottest region of the system is no longer at the centre, but has moved nearer the surface, so that the same total heat flux through the surface can be maintained from a lower maximum temperature T_m and a lower temperature T_c at the centre than in the absence of convection. The average temperature gradient near the surface is the same as before, but the heat flow to

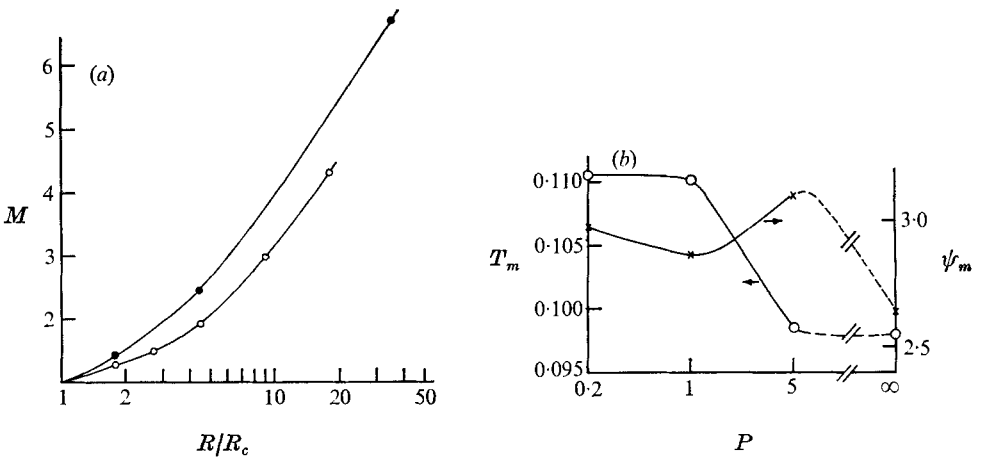

FIGURE 3. Quantitative effect of varying (*a*) the Rayleigh number R and (*b*) the Prandtl number P on single-cell flows with Taylor number $\Lambda = 0$. Plotted are the thermal efficiency M, maximum temperature T_m and the maximum of the stream function ψ_m (measuring average flow speed). Results at $P = \infty$ (upper curve in (*a*)) are from Hsui *et al.* (1972).

the surface is quicker than in the absence of convection, so the temperature of the fluid is not raised so much by the internal heating. For example, the heat generated at the centre can now escape by advection as well as by conduction, so that the temperature gradient needed for conduction falls, and with it the value of T_c. For a given form of convection cell, the parameter

$$M = T_e(0)/T_c \tag{24}$$

gives a reasonable measure of the efficiency of convection.

Figure 3(*a*) shows how M increases with R/R_c for single-cell flows, both when $P = 1$ (present results) and when $P = \infty$ (results of Hsui *et al.*). As the Rayleigh number increases, the heat flux through the surface becomes increasingly anisotropic; it is concentrated in a thermal 'boundary layer' between the temperature maximum and the surface, where the temperature gradient has increased from its conductive value. As this boundary layer gets thinner, so the number of mesh intervals spanning it decreases, and therefore so does the accuracy of the numbers computed. With 16 mesh intervals between the centre and the surface, when $R \sim 20R_c$ the temperature can reach $0{\cdot}4T_m$ at the first internal grid point and $0{\cdot}7T_m$ at the second. Therefore, not much weight can be given to the actual numbers in the calculations of Hsui *et al.* with $R \sim 50R_c$ and even fewer mesh points, though their qualitative picture is probably correct.

The contours of ζ' reflect the relative importance of advection and diffusion in the dynamics of the flow. For a single-cell mode, the solution of the linear equations (with zero advection) has ζ' falling off smoothly from a maximum at the centre. At the other extreme, as the Reynolds number of the flow tends to infinity, the variation of ζ' is concentrated near the edges of the flow and ζ' is effectively constant over most of the sphere (Batchelor 1956). (This behaviour,

suggested by (16), is why contours of ζ' are presented rather than ζ or $Q = \zeta rs$.) The flow of figure 2(*a*) lies between these extremes; the advection and diffusion terms in (13) are of about equal magnitude.

4.2. *Uniqueness of the solutions with* $P = 1, \Lambda = 0$

Like those of Hsui *et al.* (1972) the present computations yield a stable single-cell solution at all Rayleigh numbers considered. That is, this solution, once it has grown, is stable to small or moderate ($\sim 20\,\%$) perturbations from other modes. For sufficiently high Rayleigh numbers, however, other stable solutions are also possible, even with a stress-free boundary, although Hsui *et al.* make no mention of them.

In particular, at $R = 10000$, I find a stable two-cell solution with cold fluid falling at the equator (which will be referred to as the '$2E$' mode), and at $R = 40000$, there is also a two-cell solution, but with matter falling at the poles (the '$2P$' mode). These flows are shown in figures 2(*b*) and (*c*) respectively. The reverse flows ($2P$ at $R = 10000$ and $2E$ at $R = 40000$) are unstable. That is, a weak, or even a fully developed, flow of such a form spontaneously evolves into one of the stable forms. This sometimes requires a change of horizontal scale; contrary to a view sometimes expressed, such changes can and do take place in two-dimensional numerical experiments, and do not necessarily require an intermediate three-dimensional stage. The stable flows can be obtained by starting with initial conditions of similar form to the steady state (though the initial disturbance to conductive equilibrium need not be strong). It is not necessary to make the initial disturbance a pure eigenfunction of the linear equations, as long as it contains an appreciable component of the desired solution. As noted by Foster (1969) in a similar context, the horizontal mode that first attains sufficient amplitude to cause nonlinear interactions such that the temperature field is modified to fit it will be 'locked-in' and will dominate the flow pattern. A mode may win the race to nonlinearity either by being the fastest growing or by having larger initial amplitude. For $R \gg R_c$, many modes have large positive growth rates (according to linear theory) and the effect of initial conditions will be decisive. Such dependence on initial conditions has been found in many other studies of convection, both experimental (Krishnamurti 1970) and theoretical (Young 1974), and elsewhere in hydrodynamics (Segel 1966).

The direction of flow is not predicted at all by the linear or mean-field equations (Baldwin 1967), which are invariant under change of sign. By inspection of solutions like those of figures 2(*a*) and 4(*c*), one sees that, for the odd modes (i.e. those with horizontal wavenumber $l = 1, 3, 5, \ldots$), the essential topology of even the developed flow remains the same whether the flow is northwards or southwards along the axis. The two cases are mirror images (reflected about the equator $\theta = \frac{1}{2}\pi$), and it is easy to show that if one satisfies the equations of motion then so does the other. For the even modes this is not true, as can be seen by comparison of the flows of figures 2(*b*) and (*c*): one has a single maximum of temperature near the equator, the other has two near the poles.

In the range where two-cell flows occur, the present results indicate that the

$2E$ mode is preferred at low Rayleigh numbers and the $2P$ mode at higher R. This behaviour is largely caused by the imposed axisymmetry, and is most easily understood by considering the matter falling from the cold outer surface. The cold boundary dominates the behaviour of the system, because it is the origin of the non-uniformities in the flow (everywhere else being uniformly heated), and it is there that the horizontal temperature gradients $\partial T'/\partial\theta$, which drive the motion, are established as the thermal boundary layer 'peels off'. In an axisymmetric flow, when matter falls at the equator it falls in a broad 'sheet' extending round the circumference, which enables a greater volume of cold fluid to be carried down from the boundary than in the alternative $2P$ configuration, when it falls from the poles in thin columns. In the $2P$ mode, on the other hand, the cold matter descends in a column along the axis, and cannot be shaken so easily by an axisymmetric perturbation, so the $2P$ mode is preferred at large R.

4.3. *Effect of Prandtl number when* $\Lambda = 0$

As indicated by figure 3(*a*), my computed flows show only a gradual variation with Rayleigh number, so to investigate the effect of Prandtl number, it suffices to examine solutions at one typical Rayleigh number. I therefore computed the single-cell solutions at $R = 10000$ for $P = 0{\cdot}2$, 1 and 5, a range of P which allows a dramatic variation in the flow with $\Lambda > 0$ (§§5 and 6 below). The computed velocity and temperature fields all looked very similar to that of figure 2(*a*), and also to that of figure 2 of Hsui *et al.* (1972), which shows their solution with $P = \infty$, $R = 10000$. (The computed vorticity fields show more variation, but solving (17) smooths out the differences.) Figure 3(*b*) shows that, compared with the flow of Hsui *et al.*, my flows with finite P use more kinetic energy (measured crudely by $\psi_{\max}$) and lower distortion of the temperature field (measured by $T_{\max}$) to transport the same amount of heat to the surface. This is the trend reported by Veronis (1966*a*) in his numerical study of Rayleigh–Bénard convection. The present results with $P = 5$ might be expected to agree well with those of Hsui *et al.* with $P = \infty$, and indeed we do find almost the same values for T_m and T_c. But the former have ψ about 20% larger than the latter, even though the stream function with $P = 5$ (not shown) is rather more symmetric about the equator, so that the total kinetic energy of the two flows may well be about the same, with the asymmetric flow of Hsui *et al.* having higher velocities in one hemisphere and lower velocities in the other.

The two-dimensional numerical experiments of Moore & Weiss (1973) on Bénard convection suggest that the Prandtl number could be lowered indefinitely without greatly affecting the present computed flows, but laboratory experiments (Krishnamurti 1970) suggest that three-dimensional time-dependent convection would occur in practice.

5. Results with non-zero rotation and 'large' Prandtl number

To obtain examples of flows dominated by viscous effects, even when a substantial overall rotation is present, we look at the case $\Lambda \sim 10^3$, $P = 5$. In order to examine as wide a range of R, Λ and P as possible I have used the available

computing time to compute many cases at moderate resolution (16×16; see figure 1), rather than a few at high resolution (e.g. 50×50). The computations are therefore restricted to $R \lesssim 20R_c$, because to resolve adequately the thermal boundary layer when $R \gtrsim 20R_c$ would require substantially more than 16 points in r. The Taylor number is similarly restricted to the range $0 \leqslant \Lambda \leqslant 4 \times 10^3$ by truncation errors, which manifest themselves most obviously in the form of spurious angular momentum entering through the nominally 'stress-free' surface. This spurious angular momentum becomes unacceptably large in well-developed flows with larger (R, Λ) than are dealt with here.

5.1. *Onset of instability*

For $\Lambda = 200$ and $\Lambda = 1000$, the critical Rayleigh number found in these numerical experiments was within 1 % of the value predicted by the linear calculations of Roberts (1968). For $\Lambda = 4000$, instability set in at $R = 13{\cdot}0 \times 10^3$ compared with Roberts' value of $R = 12{\cdot}0 \times 10^3$. This discrepancy may reasonably be attributed to truncation errors in my program, the effect of which may be expected to increase with Λ. For, at a given growth rate, as Λ increases, we are looking at the same small difference but between increasingly large terms in (13), which is the formal reason why R_c increases with Λ. Therefore an error which is a fixed proportion of one of the terms will have an increasing effect as the terms themselves increase with Λ.

Other results that agree with linear stability theory are the absence of overstable (growing oscillatory) modes when $P = 5$, and the measured growth rates of modes other than $l = 1$. Both Roberts' linear calculations and the present results show the odd modes to be more unstable than the even at most Taylor numbers, but that at $\Lambda = 1000$ both are almost equally unstable.

5.2. *Steady flows with* $P = 5$, $\Lambda > 0$

Stability calculations indicate that the complexity of the flow increases rapidly with Λ: the marginally stable state involves increasingly many spherical harmonics (Bisshopp 1958). This tendency may be clearly seen in the fully developed steady flows shown in figure 4, all of which were started from a weak single-cell disturbance, and have $R \lesssim 3R_c$. We see that the preferred mode is a single cell for weak rotation ($0 \leqslant \Lambda \leqslant 200$), a double cell ($2E$) for moderate rotation ($\Lambda = 1000$) and a triple cell for larger rotation ($\Lambda = 4000$). For greater R/R_c the situation is more confused because more than one stable flow is possible, as discussed below, but the prevailing tendency is still for the wavenumber l to increase with Taylor number Λ as indicated in figure 1 (*b*).

The tendency for the number of cells to increase with Λ reflects the way in which rotation constrains convection: motions perpendicular to the axis are inhibited by Rayleigh's angular-momentum criterion (Chandrasekhar 1961, § 66). Therefore as Λ increases the convection cells are compressed in the direction perpendicular to the axis, so that each fluid particle does not have to move so far perpendicular to the axis; if the rotation is strong enough, axisymmetric flow will tend to take the form of a succession of cells one outside the other. The flow

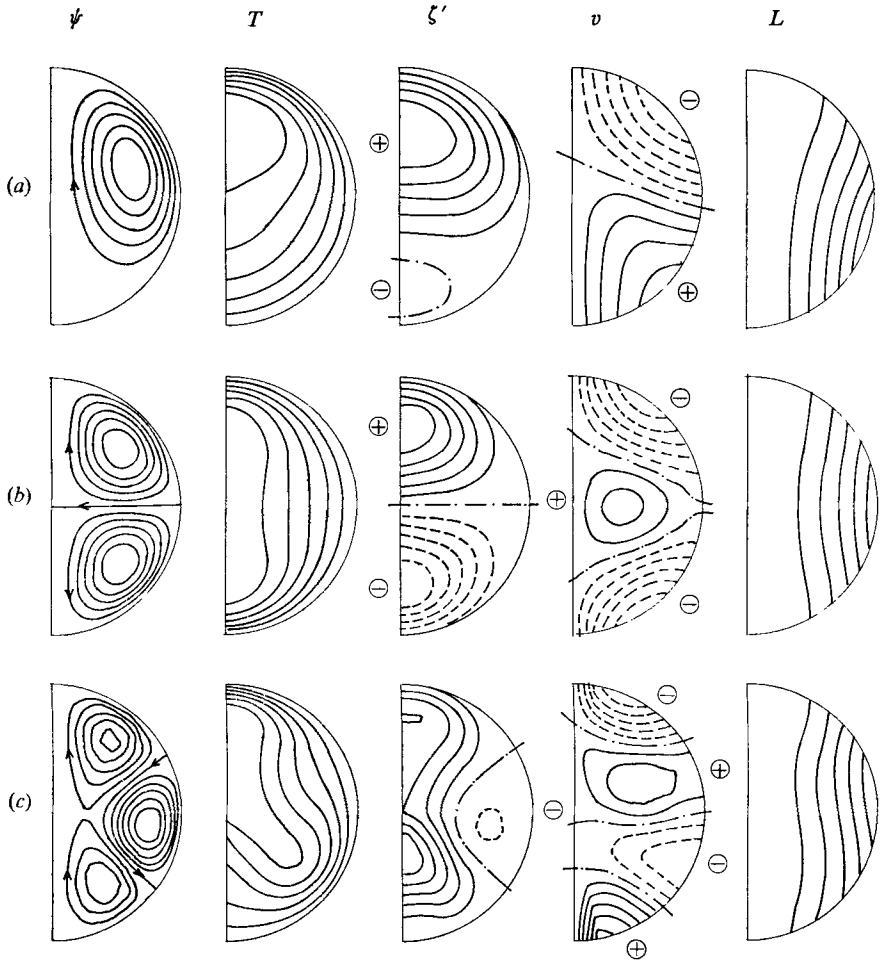

FIGURE 4. Effect of increasing Taylor number Λ on steady axisymmetric convection in a rotating fluid sphere with Prandtl number $P = 5$ and Rayleigh number $R \lesssim 4R_c$. Conventions as in figure 2; v is the azimuthal velocity (relative to the initial uniform rotation Ω), $L = v\varpi + \Omega\varpi^2$ is the angular momentum per unit mass. All started from a single-cell perturbation to static equilibrium. Note the increase in wavenumber with Λ.

	Λ	R	R/R_c	max ψ	max T'	max ζ'	max v	max L
(*a*)	200	8000	2·6	1·00	0·128	102	12·3	36·7
(*b*)	1000	10000	1·5	0·845	0·113	235	12·6	73·3
(*c*)	4000	30000	2·5	1·41	0·107	728	29·2	160

of figure 4 (*c*), with $l = 3$, is showing this tendency, but the present computations do not extend to high enough Λ to show it more dramatically. Non-axisymmetric convection is likewise compressed perpendicular to the axis, into the form shown by Busse (1970*a*).

We see that, once the flow has developed, it distorts the initially spherically symmetric temperature distribution as in §4. Figure 5 shows a plot of thermal efficiency $M = T_e(0)/T_c$ against R/R_c for some typical flows. Note that the

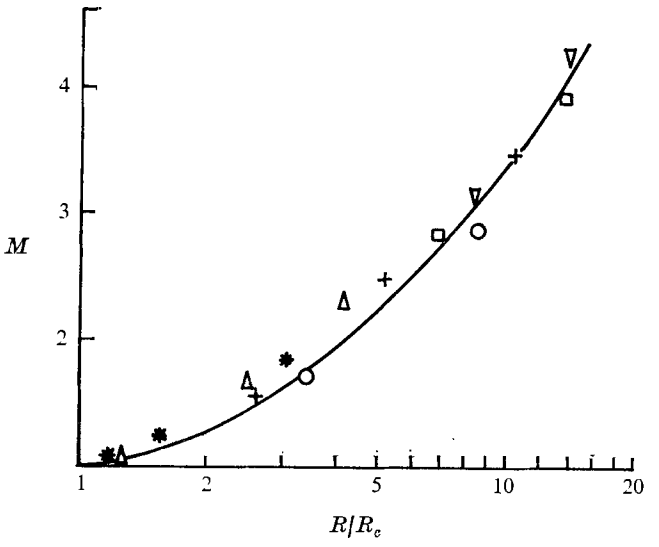

FIGURE 5. Thermal efficiency $M = T_e(0)/T_c$ against Rayleigh number. For $P = 5$ abscissa is R/R_e; for $P = 0{\cdot}2$ it is R/R_0 (cf. figure 1).

	+	*	△	○	□	▽
Prandtl number, P	5	5	5	0·2	0·2	0·2
Taylor number, Λ	200	1000	4000	200	1000	4000
Wavenumber, l	1	$2E$	3	1	1	1

strength of the convection is fairly well predicted by R/R_c and depends only weakly on Λ. This reflects the success of calculations of convection based on expansions in $\epsilon = [(R/R_c) - 1]^{\frac{1}{2}}$ such as those by Veronis (1959). For given (Λ, R), figure 5 shows only the mode with the highest M, which here turns out to be that selected by the marginal-stability equations.

The distortion of the total angular momentum L from the initial cylindrical configuration measures the azimuthal velocity v. In the flow of figure 4(*b*), for example, fluid of low angular momentum is pushed out from the axis in high latitudes, to form regions of negative v. Figures 4(*b*) and 6(*b*) show that the $2E$ mode produces an equatorial acceleration and the $2P$ mode an equatorial deceleration. In the single-cell solution of the linear equations, the equator is a line of $v = 0$. The increasing departure from this as R/R_c increases from figure 4(*a*) to figure 6(*a*) reflects the increasing strength of the nonlinear terms in (15). Nevertheless in the flows shown in figures 4 and 6 the distortion of L from its initial cylindrical configuration is not large, which implies that $L_3 \equiv v\varpi$ (that part of the angular momentum which has been transported by the meridional circulation) is sizeably less than the initial part $L_0 \equiv \Omega\varpi^2$. But in calculations with $P = 5$ and $R \gtrsim 10R_c$, where the meridional circulation is much stronger, it can happen that $|L_3| \gtrsim L_0$. In such calculations, it was found that appreciable spurious angular momentum had entered the system, because of the discretization errors at the surface mentioned in §3; the parameter

$$e_L = \int v\varpi \, dV / \int \Omega\varpi^2 \, dV, \tag{25}$$

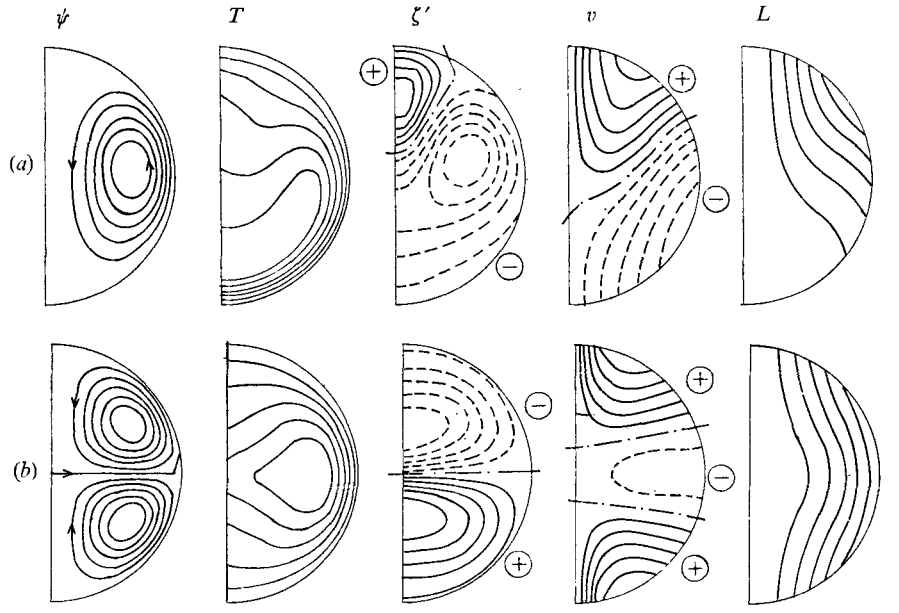

FIGURE 6. Steady flows at higher R/R_c with $P = 5$, $\Lambda > 0$. Conventions as in figure 4.

	Λ	R	R/R_c	max ψ	max T	max ζ'	max v	max L
(*a*)	1000	40000	6·4	5·33	0·078	325	51·3	68·8
(*b*)	200	16000	5·2	2·05	0·089	350	18·4	30·9

which would be zero if angular momentum were perfectly conserved by the numerical scheme, reached the unacceptable level of $|e_L| \gtrsim 0{\cdot}2$ before even a quasi-steady state had been established.

For flows with lower (R, Λ) this leak of angular momentum still existed, but was sufficiently slow that a quasi-steady state formed after 3 or 4 turnover times. Such quasi-steady solutions, of which those in figures 4 and 6 are examples, have $|e_L| \lesssim 0{\cdot}04$ and should be a good approximation to the true steady solution of the analytic equations. If the computation continues forward in time from a quasi-steady state, the parameter e_L changes monotonically by $\sim 2\%$ per turnover time, while the meridional fields ψ and T change rather more slowly. For a $2P$ flow, $e_L > 0$; for a $2E$ or single-cell flow, $e_L < 0$.

Just as the form of v reflects the balance of terms in (15), so the form of ζ' reflects the balance in (13), and in particular the importance of the nonlinear term div $(\mathbf{u}\zeta')$ in (16). Thus in the flow of figure 6(*a*), with $R = 6{\cdot}2R_c$, the maximum of ζ' has been carried further from the centre of the sphere than in that of figure 4(*a*), with $R = 2{\cdot}6R_c$. No solutions in which advection of vorticity dominates the other processes have been computed with $P = 5$, because they would have strong meridional circulations and therefore be unrealistic because of poor numerical conservation of angular momentum.

Numerical experiments can separate the individual terms in the equation of motion, thus giving insight into the dynamic balances in the flow. We find that

in all the present flows there is a local balance of terms: the viscous terms grow to meet whatever challenge is thrown at them, as in the 'viscous regime' of Moore & Weiss (1973). (In contrast, in their 'advective regime' (of large R and small P) the advection of vorticity was so strong that a fluid element could go several times round a cell before being seriously retarded by viscous forces.) The scale of the terms in (13) is set by the buoyancy term $-(g\alpha/r)(\partial T/\partial\theta)$, which is a maximum where the thermal boundary layer peels off the outer surface (where $\partial T/\partial\theta$ is large) and a minimum near the centre (where g is small).

The direct effect of rotation on the meridional flow, as measured by the terms proportional to Ω in (13), increases with the Taylor number Λ. In the flow of figure 4(*a*), with $\Lambda = 200$, the rotation terms are important in the dynamical balance only near the equatorial surface, where $\boldsymbol{\Omega}.\nabla v$ is a maximum and the buoyancy terms are small because $\partial T/\partial\theta = 0$ at the surface. Elsewhere the magnitude of the rotation terms is less than 20% of the buoyancy terms; the dominant balance is between the latter and viscous diffusion. In the flow of figure 4(*c*), on the other hand, $\Lambda = 4000$ and the rotation and diffusion terms have roughly equal inhibiting effect on the vorticity created by the horizontal temperature gradients. In this flow, both ζ and ψ are almost directly proportional to $g\partial T/\partial\theta$, which shows how weak is the influence of advection of vorticity.

5.3. *Effect of initial conditions when* $P = 5, \Lambda > 0$

Most of these computations were started by imposing a weak single-cell meridional circulation on an (unstable) state of conductive equilibrium, and the results show that a single-cell flow cannot be sustained for sufficiently strong Λ (see figures 1(*b*) and 4). But, as in §4, at certain (Λ, R) a range of stable solutions can be produced by using suitable initial conditions, while modes not included in this limited range cannot be sustained at that (Λ, R). For example, at $\Lambda = 200$, $R = 16000$, there are precisely three stable solutions: the $2P$ flow shown in figure 6(*b*) and a $2E$ flow and a single-cell flow like those of figures 4(*b*) and (*a*) respectively.

Of the two-cell flows the $2E$ mode is preferred at low R and the $2P$ at high R, as when $\Lambda = 0$. The explanation for this behaviour given in §4 is reinforced by considerations of angular momentum. In the $2P$ mode, fluid of low angular momentum is transported towards the surface at the equator (as in figure 6*b*), so near the centre $\partial L/\partial\varpi$ is decreased from its original value, whereas it is increased near the surface, thereby stabilizing the outer regions against interchange instabilities according to Rayleigh's criterion (Chandrasekhar 1961, §66). For given Λ, such angular-momentum instabilities become more of a threat to stability of a finite amplitude solution as v increases, i.e. as R increases, and the $2E$ mode is less stable to them than the $2P$, giving another reason why the $2P$ mode is preferred at high R.

6. Results with non-zero rotation and 'small' Prandtl number

All the results in this section were obtained with a Prandtl number $P = 0{\cdot}2$. The results indicate that this is sufficiently small to be typical of the range of P for which Coriolis and inertial forces dominate viscous effects, producing remarkable differences from the flows of §5. A few flows computed with $P = 1$ showed very similar behaviour to those with $P = 0{\cdot}2$. The range of (R, Λ) covered (figure 1*b*) is governed by the factors listed in §5.

6.1. *Onset of instability*

As indicated by figure 1(*c*), the present study shows that, when $P = 0{\cdot}2$, a small disturbance to conductive equilibrium can grow as an oscillatory mode at Rayleigh numbers below those for which monotonic growth can occur. The critical Rayleigh number $R_0(\Lambda)$ for the onset of this instability was found by extrapolating to zero the real part of the measured growth rate of a single-cell disturbance, giving

$$\left.\begin{aligned} R_0(200) &= (2{\cdot}35 \pm 0{\cdot}1) \times 10^3, \\ R_0(1000) &= (2{\cdot}9 \pm 0{\cdot}1) \times 10^3, \\ R_0(4000) &= (3{\cdot}6 \pm 0{\cdot}2) \times 10^3, \end{aligned}\right\} \tag{26}$$

where the uncertainties come from difficulties in measuring the growth rates, since the periods of oscillation involved are $\gtrsim 2\,(r_0^2/\kappa)$.

Earlier linear stability calculations for the present model (Roberts 1968) did not encompass overstability for technical reasons, but the stability theory of a rotating plane layer heated from below (Chandrasekhar 1961; Weiss 1964) indicates that overstability should occur for sufficiently low P and high Λ. Such oscillations can occur only in a fluid of low Prandtl number, because, in a more viscous fluid (e.g. one with $P = 5$), the characteristic time $\tau_\nu = r_0^2/\nu$ for viscous forces to take effect is sufficiently short that viscosity can set up a local balance of forces before oscillation can occur. The theory also suggests that, for a given configuration and given P, the period of overstable oscillations should increase as Λ decreases down to some limit $\Lambda_0(P)$, below which overstability cannot occur. This trend was found in the present results, which indicate that $\Lambda_0(0{\cdot}2)$ is not much below 200 (see figure 1*c*).

Unsuccessful attempts were made to produce a steady subcritical solution of the form described by Veronis (1966*b*), by taking a steady solution at some (Λ, R) as the initial condition for a run at (Λ, R') with $R_0 < R' < R_e$.

6.2. *Steady flows with* $P = 0{\cdot}2$, $\Lambda > 0$

For sufficiently high R, steady solutions are obtained with $P = 0{\cdot}2$ and $\Lambda = 200$, 1000 and 4000 (figure 1*c*). All of them have the same flow pattern, which is shown in figure 7 and is strikingly different from those of figures 4 and 6, which have $P = 5$.

The most striking feature of the flow is the great distortion of the angular-momentum distribution: the initial state of constant angular velocity has been

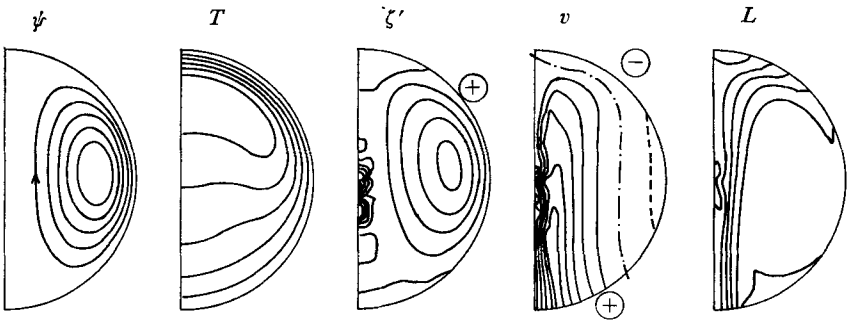

FIGURE 7. Steady convection with $P = 0{\cdot}2$, $\Lambda = 1000$, $R = 20000$. Note the distribution of angular momentum L, characteristic of $\Lambda \gg 1, P \ll 1$. Maximum values of each variable: ψ, 4·92; T, 0·0836; ζ', 278; v, 7·96; L, 1·82.

changed into one of nearly constant angular momentum. The angular momentum has been redistributed by the single-cell meridional circulation; fluid of low angular momentum is brought from near the north pole to the equator, and fluid of high angular momentum is taken from near the equator and transported to near the south pole, which results in an almost uniform distribution of angular momentum throughout the system. It is possible for angular momentum to be advected because the viscosity is low enough that a fluid particle can retain most of its angular momentum as it moves over a considerable distance.

In terms of the zonal velocity v, the initially antisymmetric distribution has been sheared round by the meridional circulation in the same way as for $P = 5$, but because the opposing viscous forces are weaker, the contour $v = 0$ can be sheared until it is at right angles to its initial location at $\theta = \frac{1}{2}\pi$, rather than the modest inclinations reached when $P = 5$ (compare figure 7 with figure 6*a*).

The basic reason for this behaviour is as follows. The system would like to convect, in order to get its heat out more efficiently, but is restrained from so doing by Rayleigh's angular-momentum criterion (Chandrasekhar 1961, §66). An axisymmetric fluid element can move outwards only if it acquires the angular momentum appropriate to where it wants to go. If the viscosity is high, then it acquires the necessary angular momentum by viscous transfer from neighbouring fluid elements (as in the flows with $P = 5$), but if the viscosity is low (as here) it is easier for the system to create a region where the angular momentum is nearly constant, so that this constraint on the motions no longer applies.

Another striking feature of the computed flows is that they differ only quantitatively from one another; all show the characteristic distribution of angular momentum, and have the single-cell structure necessary to maintain it. Attempts to create a multi-cell flow, by varying the initial condition from the usual weak single cell, were unsuccessful; the cell form shown in figure 7 appears to be the only stable solution for the (R, Λ, P) concerned. Further, the physical argument presented above strongly suggests that this cell form, with its characteristic distribution of angular momentum, will be strongly preferred to other axisymmetric modes for all lower P, higher Λ and higher R.

Because of this uniqueness of form, it is sufficient to discuss only one typical

flow in detail: we shall specifically consider that with $\Lambda = 1000$, $R = 20000$ (figure 7), but most of the remarks apply to the other computed flows.

The stream function and temperature fields resemble qualitatively those one would expect for a single-cell flow of medium strength. Figure 5 illustrates the quantitative agreement between all the computed single-cell flows. The flow strength M is almost 'independent' of Λ and P and depends only on the form of the meridional motion and on R/R_c, provided one takes $R_c = R_0$ for the points with $P = 0{\cdot}2$.

The vorticity distribution reflects the importance of advection of vorticity: the maximum of ζ' lies near the surface, rather than near the axis (cf. figure 6*a*). Note that (16) implies that for steady flow of an inviscid fluid in an isothermal region

$$\mathbf{u}.\nabla\zeta' = 0, \tag{27}$$

which means that ζ' is constant along streamlines, a situation not so very different from that found here (Batchelor 1956). Near the surface at the equator, where the velocities are greatest (look at ψ), advection of vorticity contributes at least as much to the balance (13) as do the buoyancy forces, and the two are balanced locally by viscous diffusion. The term $2\boldsymbol{\Omega}.\nabla v$, representing the constraining effects of rotation, is small over most of the flow, because v is constant along axial cylinders. This is the formal expression of the angular-momentum argument presented above.

Although the angular momentum L is constant over most of the flow, there is a steep gradient in L near the axis, caused by fluid of high angular momentum being pushed into a small cylindrical region surrounding the axis. Mathematically, this gradient (and also the similar gradient in v) is caused by the boundary condition (21), i.e. $v = 0$ at $\varpi = 0$, imposed to avoid having an infinite angular velocity v/ϖ at the axis. This distribution of L, with its concentration of 'field lines' near the axis, resembles the distributions of magnetic field around an eddy suggested by Parker (1963) and found in numerical experiments by Weiss (1966) and Peckover & Weiss (1972).

Gough & Lynden-Bell (1968) have pursued this analogy and argued that, although Rayleigh's criterion favours a state of strictly uniform L, this would imply a singularity at the axis, unless $L = 0$, and therefore that, in practice, the convecting region would expel its angular momentum to other parts of the system, in analogy with the expulsion of magnetic field studied by Weiss. However, I think it more likely that the system would avoid a singularity at the axis by allowing a gradient in L in a small surrounding region, as in figure 7, though the present model cannot exclude the expulsion hypothesis, because the convecting region in the model is bounded by a stress-free surface, through which (in principle) no angular momentum can pass. A more elaborate model, in which this possibility is not excluded, is presented by Weir (1975), together with some preliminary results which suggest that, in fact, angular momentum is not expelled.

Note that, despite the large changes in the distribution of angular momentum, the numerical scheme has conserved the total angular momentum of the system reasonably well: the flow in figure 7 has $e_L = -0{\cdot}06$ although $|e_L|$ is slowly

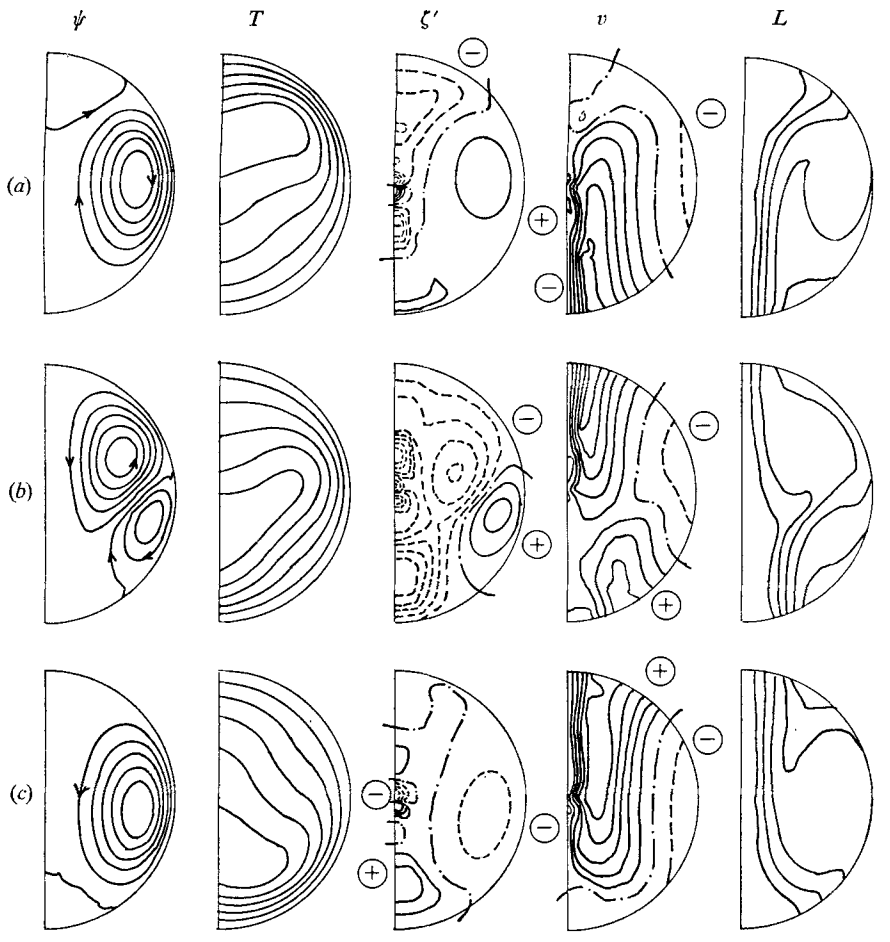

FIGURES 8(a–c). For legend see facing page.

increasing with time, as described in §5.2. The computed zonal velocity field v has kinks near the centre, where $r = s = 0$ and the truncation errors in (A 4) are $O(h\delta)$ and becoming comparable to the true terms. These effects are particularly great in the advection and diffusion terms, which involve the highest powers of ϖ (in forms like $\varpi^{-n}\partial(\varpi^n f)/\partial\theta$). But the fictitious angular momentum $v\varpi$ manufactured thereby is numerically not very large and comes from only a very small proportion of the total volume (or mass) of the system, and so its contribution to the total angular momentum of the system should be negligible.

Away from the axis (say, for $r > \frac{1}{2}, \sin\theta > 0{\cdot}1$), viscous diffusion of angular momentum is small, and the balance in (15) is primarily between the Coriolis force and advection of angular momentum. Diffusion ensures a local balance, but is relatively small over most of the volume (less than 20 % of the Coriolis terms).

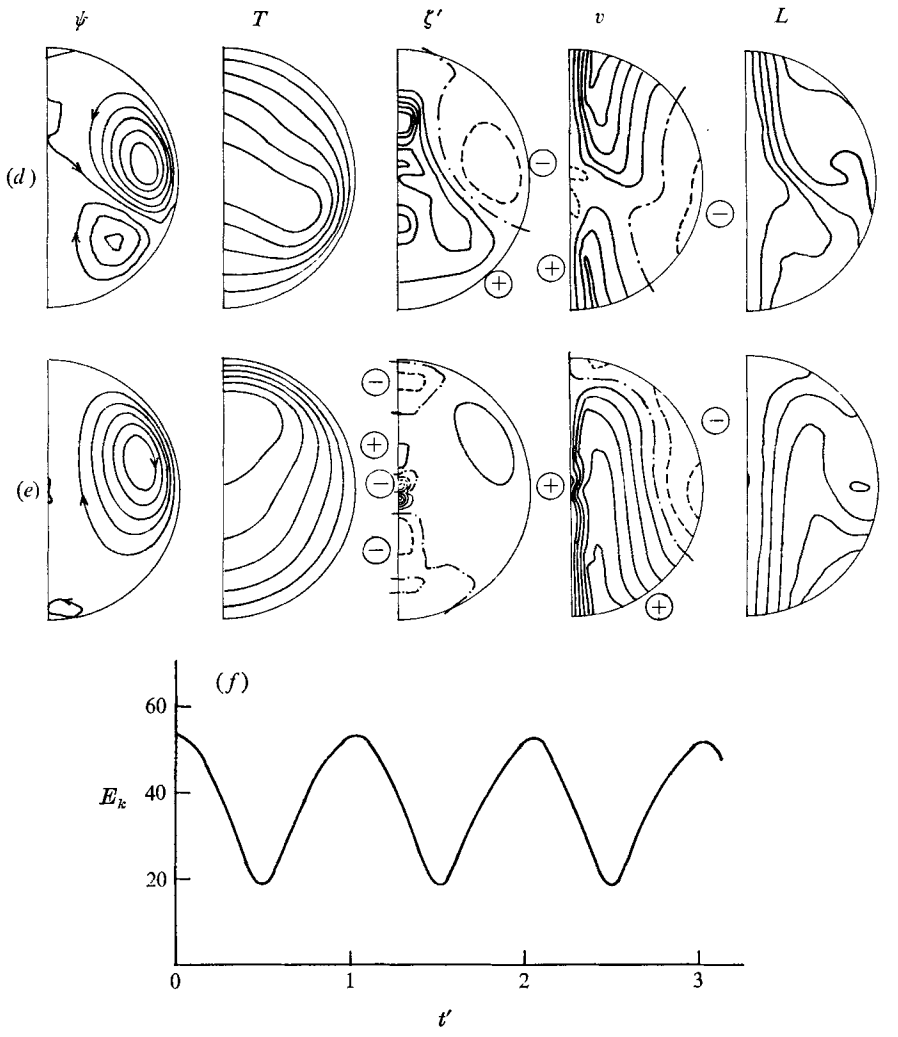

FIGURE 8. Oscillatory solution with $P = 0{\cdot}2$, $\Lambda = 4000$, $R = 15000$ at various times t'. Unit of time is r_0^2/κ, origin of t' is arbitrary, period of oscillation is 2·0 units.

	t'	max ψ	max T	max ζ'	max v	max L
(*a*)	0	3·30	0·102	754	14·0	4·55
(*b*)	0·4	1·72	0·114	291	10·9	5·04
(*c*)	0·8	2·99	0·119	699	10·0	5·02
(*d*)	1·2	2·39	0·099	565	14·8	4·80
(*e*)	1·6	2·48	0·130	669	10·6	5·43

(*f*) Kinetic energy E_k as a function of time t' (with $t' = 0$ corresponding to (*a*)).

6.3. *Sustained oscillatory flows*

As indicated in figure 1(*c*), a Prandtl number of 0·2 is sufficiently low that oscillatory flows can be sustained over a range of R. These are the well-developed versions of the overstable modes of §6.1, and have all been followed from their start as a single weak cell.

Figure 8 shows one such case (with $P = 0{\cdot}2, \Lambda = 4000, R = 15\,000$) after it has settled down, having already gone through about 5 periods of oscillation. The pattern repeats itself regularly, as nearly as can be ascertained, but it is likely that, after another 10 or 20 cycles, truncation errors would allow sufficient spurious angular momentum to enter through the nominally stress-free boundary to destroy the regularity.

The oscillation arises essentially because the Rayleigh number is too low for the buoyancy force to overcome completely the rotational constraint. As the buoyancy forces build up ζ and ψ, so the Coriolis forces increase v and build up the rotational constraint $2\boldsymbol{\Omega}.\nabla v$ to such an extent that it can actually reverse the motions. As the motion reverses, v falls and the cycle repeats itself.

Figure 8(f) shows the variation of kinetic energy with time for this flow. For simple harmonic motion, where the inertial (nonlinear) effects are negligible, this graph would be sinusoidal with $E_k = 0$ once every half-period. For oscillations primarily due to inertial effects (e.g. those described by Moore & Weiss 1973), the kinetic energy does not vary by more than 10 or 20 % in the course of an oscillation and the graph of E_k against time can be highly non-sinusoidal. In the present case, E_k varies nearly sinusoidally with time, but falls not to zero, but to about half its mean value, indicating that inertial effects are significant but not dominant. Indeed, it transpires that the average magnitudes of the buoyancy, advection and diffusion terms in (13) are roughly equal.

The flow of figure 8 has $R > R_e$, the Rayleigh number at which the 'exchange of stabilities' takes place, and for such cases, stability theory predicts that small disturbances to conductive equilibrium must grow monotonically rather than as oscillations (Weiss 1964). This oscillatory solution exists because inertial effects reinforce the restoring effect of the Coriolis forces. For example, the inertia in the azimuthal motions leaves v still creating negative ζ (as in a steady flow with positive ζ) even when ζ has become negative over most of the flow. The redistribution of angular momentum is not sufficient to nullify the rotational constraint, though at each peak of kinetic energy (e.g. at $t' = 0$), the flow looks remarkably like the steady flow of figure 7.

Related to the importance of the inertial terms in this flow is the remarkably large amplitude of the motions: the convection cell turns over about four times in each period. For flows with lower R/R_0, the amplitude is of course much smaller, declining to zero as $R \to R_0$.

7. Application to stars

Many stars are known to be rotating, and this markedly affects their structure, luminosity and evolution (see, for example, Fricke & Kippenhahn 1972). Calculations by Bodenheimer (1971) and others suggest that the observable luminosity and temperature of a normal (i.e. main-sequence) star depend only on its mass M and total angular momentum J, and are independent of the precise way in which the angular velocity varies within it. Unfortunately, J cannot be observed directly, and to compare theoretical models of stars with observations one has to infer J from V, the observed surface velocity at the equator, and to do so one

needs to know the internal law of rotation. Bodenheimer's results show that for given M and V the predicted luminosity can vary by at least a factor of two depending on which of several plausible rotation laws is assumed.

The most common assumption about the internal rotation of a star is that it is uniform, but Tayler (1973) suggested that (for stars sufficiently massive to have a convective core) a more consistent procedure would be to derive the rotation law in the core from the dynamics of convection and to deduce the law in the outer regions from that. He also gave heuristic arguments based on the mixing-length model of convection that suggested that the angular momentum per unit mass, rather than the angular velocity, would be constant in the core. One motivation for the present study was to see to what extent large-scale convection (as distinct from the secondary circulations described by Tayler) could redistribute angular momentum, and in particular whether the distribution hypothesized by Tayler could arise.

The present model does have the basic geometry of a stellar core, and the steady flows of §6, with $P \ll 1$ and a stress-free outer surface, do indeed have the specific angular momentum nearly uniform throughout the 'core', as hypothesized by Tayler, but how well does the model resemble a real convective core? The qualitative features of the flow should be independent of details like the Boussinesq approximation and the neglect of the centrifugal force. The 'molecular' Prandtl number in a star is of order 10^{-6}, and even that based on eddy viscosity and conductivity (parameterizing the smaller scales of motion) should be $P_e \sim 1$, which still gives constant L in the model. A stress-free boundary condition is clearly more realistic in a star than a rigid one (which suppresses the redistribution of L), though to allow explicitly for the overlying stably stratified region would be even better. Preliminary results with a model that does so (Weir 1975) indicate that the distribution of angular momentum in the model core is not greatly changed from that of §6: the expulsion of angular momentum suggested by Gough & Lynden-Bell (1968) does not take place. The assumption that the dominant length scale of the convection is comparable to the depth of the core may be justified by the argument that the largest scales are the most efficient (Simon & Weiss 1968), by mixing-length theory (which takes the scale as the local pressure scale height, which is of the same order as the depth of the core; Schwarzschild 1958, p. 254), and by the numerical experiments of Graham (1975).

For the moderate Taylor numbers explicitly examined in §§5 and 6, the stability theory of Roberts (1968) indicates that axisymmetric modes may be marginally preferred, as the tendency of rotation to compress the horizontal scale of the motion (Veronis 1959) has not become strong enough to overcome the natural tendency of convection to have its horizontal and vertical scales comparable (Rossby 1969). But, because of the huge lengths involved, the Taylor number of a stellar core is at least three powers of ten larger, even when based on eddy viscosity, and the stability theory for such high Λ (Roberts 1968; Busse 1970*a*) indicates that marginal convection takes the form of a ring of thin cylindrical rolls aligned parallel to the axis, with azimuthal wavenumber $m \sim \Lambda^{\frac{1}{2}}$. Since the Rayleigh number in a star is also enormous, such marginal

solutions are not directly relevant, but unpublished† experiments by Busse & Carrigan indicate that the effect of increasing R at such high Λ is to add extra rings of rolls to the marginal flow. In such non-axisymmetric solutions, the sign of v alternates from roll to roll, ensuring a non-uniform distribution of L: the rotational constraint is overcome essentially by horizontal compression (cf. §5). But these results refer to the situation where the Rayleigh number of a static sphere is slowly increased from zero; if a large-scale circulation like that of figure 7 has already been established by some other mechanism, then thermal convection will reinforce it, since the rotational constraint is weakened already. It should be possible to perform an explicit calculation to confirm the stability of such a flow to non-axisymmetric disturbances.

I conclude therefore that, while the idea of a core of nearly uniform angular momentum has an attractive physical simplicity and has been shown in §6 to be dynamically possible, it may not be realized in practice because of the likely occurrence of highly non-axisymmetric motions.

This work was carried out in the Department of Applied Mathematics and Theoretical Physics in the University of Cambridge, where I held successive scholarships from the Australian National University and the Cambridge Philosophical Society, for which I am grateful. I thank Nigel Weiss for his sustained help and encouragement, and acknowledge helpful discussions with Herbert Huppert, John Huthnance, and Paul Gurbutt. The computations were performed on the IBM 370/165 of the Cambridge University Computing Service; I thank the Superintendent for a generous allocation of computer resources, and Peter Linington and Richard Stibbs, who wrote the plotting routines. I also thank Fritz Busse and some anonymous referees for constructive criticism of an earlier version of this paper. A preliminary account of some of these results was presented to the 19th Liège Astrophysical Colloquium (Weir 1975).

Appendix. Details of the difference schemes

We use a two-dimensional mesh with uniform spacings $h = (J-1)^{-1}$ and $\delta = \pi/(L-1)$ in r and θ respectively, and let Φ^n_{jk} denote the value of any variable Φ at the point $(r_j, \theta_k) = [(j-1)h, (k-1)\delta]$ at time $t^n = n\Delta t$.

By integrating the first three terms of (2) over the box

$$r_{j-1} \leqslant r \leqslant r_{j+1}, \quad \theta_{k-1} \leqslant \theta \leqslant \theta_{k+1}, \quad \phi_1 \leqslant \phi \leqslant \phi_1 + \Delta\phi$$

and the last term over the smaller box

$$r_{j-\frac{1}{2}} \leqslant r \leqslant r_{j+\frac{1}{2}}, \quad \theta_{k-\frac{1}{2}} \leqslant \theta \leqslant \theta_{k+\frac{1}{2}}, \quad \phi_1 \leqslant \phi \leqslant \phi_1 + \Delta\phi,$$

we obtain the following formula for updating the temperature at the interior point (r_j, θ_k):

$$\begin{aligned} V_{jk}(T^{n+1}_{jk} - T^n_{jk}) = {} & V_{jk} H \Delta t - \Delta t \{(T\Delta_\theta \psi)_{j+1,k} - (T\Delta_\theta \psi)_{j-1,k} \\ & - (T\Delta_r \psi)_{j,k+1} + (T\Delta_r \psi)_{j,k-1}\}^{n+\frac{1}{2}} \\ & + \kappa \Delta t (V_{jk}/V'_{jk}) \{(2s_k \sigma'/h)[r^2_{j+\frac{1}{2}}(T_{j+1,k} - \overline{T}_{jk}) \\ & + r^2_{j-\frac{1}{2}}(T_{j-1,k} - \overline{T}_{jk})] + (r_j \delta)^{-1}[r_j s_{k+\frac{1}{2}} h(T_{j,k+1} - \overline{T}_{jk}) \\ & + r_j s_{k-\frac{1}{2}} h(T_{j,k-1} - \overline{T}_{jk})]\}^{n+\frac{1}{2}}, \end{aligned} \tag{A 1}$$

† *Note added in proof.* A preliminary account of these experiments has recently appeared in *Science*, **191**, 81–83.

where $$V_{jk} = 4(r_j^2 + \tfrac{1}{3}h^2)\, s_k \sigma h$$
and $$V'_{jk} = 2(r_j^2 + \tfrac{1}{12}h^2)\, s_k \sigma' h \quad \text{(A 2)}$$

are the (exact) volumes of the large and small boxes,

$$\Delta_r \Phi_{jk} = \Phi_{j+1,k} - \Phi_{j-1,k}, \quad \Delta_\theta \Phi_{jk} = \Phi_{j,k+1} - \Phi_{j,k-1}, \quad \bar{\Phi}_{jk} = \tfrac{1}{2}(\Phi^n_{jk} + \Phi^{n+1}_{jk}), \tag{A 3}$$

where $$s_k = \sin\theta_k, \quad \sigma = \sin\delta, \quad \sigma' = \sin(\tfrac{1}{2}\delta),$$

and the rest of the notation is as in §§2 and 3. The unknown T^{n+1}_{jk} appears on the right-hand side in the form of $\bar{T}_{jk}$, but by simply regrouping the terms and dividing both sides by V_{jk} one obtains an explicit expression for T^{n+1}_{jk}.

Note that at each time step t^n this scheme requires us to evaluate only half the T^n_{jk}, namely those at alternate points on the mesh. The other half of the T_{jk} can then be evaluated on the next sweep, a time $\frac{1}{2}\Delta t$ or one 'half time step' later, and will suffice to update the first half at time t^{n+1}. As this applies also to the difference equations (A 4) and (A 7) for $\Delta v/\Delta t$ and $\Delta\zeta/\Delta t$, by using such a 'staggered mesh' we halve the computer time required, although the numerical solution of (17) is thereby complicated.

Thus, by integrating the ∇^2 term of (15) over V'_{jk} and the other terms over V_{jk}, one obtains

$$\begin{aligned} r_j s_k (v^{n+1}_{jk} - v^n_{jk})\, V_{jk}/\Delta t = {} & \Omega[\Delta_\theta(r_j^2 s_k^2 \Delta_r \psi) - \Delta_r(r_j^2 s_k^2 \Delta_\theta \psi)] \\ & + \Delta_\theta(r_j s_k v_{jk} \Delta_r \psi) - \Delta_r(r_j s_k v_{jk} \Delta_\theta \psi) \\ & - 2\nu\{(2s_k^2\sigma)\, \Delta_r(r_j^2 v_{jk}) + (2r_j h)\, \Delta_\theta(s_k c_k v_{jk})\} \\ & + \nu(V_{jk}/V'_{jk})\, \{(2s_k^2\sigma'/h)\, [(r_{j+1} v_{j+1,k} - r_j \bar{v}_{jk})\, r^2_{j+\frac{1}{2}} \\ & + (r_{j-1} v_{j-1,k} - r_j \bar{v}_{jk})\, r^2_{j-\frac{1}{2}}] \\ & + (r_j h/\delta)\, [s_{k+\frac{1}{2}}(v_{j,k+1} s_{k+1} - \bar{v}_{jk} s_k) \\ & + s_{k-\frac{1}{2}}(v_{j,k-1} s_{k-1} - \bar{v}_{jk} s_k)]\}, \end{aligned} \tag{A 4}$$

in which $c_k = \cos\theta_k$ and the right-hand side is evaluated at $t^{n+\frac{1}{2}}$. Again, this can be rearranged to give an explicit formula for the unknown v^{n+1}_{jk}.

To obtain a 'conservative' difference formula for ζ^{n+1}_{jk} corresponding to (13), we integrate (12) around the contour C_{jk} joining the points (r_{j-1}, θ_{k-1}), (r_{j+1}, θ_{k-1}), (r_{j+1}, θ_{k+1}) and (r_{j-1}, θ_{k+1}), except for the diffusion terms, where the integration is around C'_{jk}, joining $(r_{j-\frac{1}{2}}, \theta_{k-\frac{1}{2}})$, $(r_{j+\frac{1}{2}}, \theta_{k-\frac{1}{2}})$, $(r_{j+\frac{1}{2}}, \theta_{k+\frac{1}{2}})$ and $(r_{j-\frac{1}{2}}, \theta_{k+\frac{1}{2}})$. We shall need values of

$$\begin{aligned} \nabla \times \boldsymbol{\omega} &= \left(\frac{1}{rs}\frac{\partial(\zeta s)}{\partial\theta}, -\frac{1}{r}\frac{\partial(\zeta r)}{\partial r}, \frac{1}{r}\frac{\partial(r\eta)}{\partial r} - \frac{1}{r}\frac{\partial\xi}{\partial\theta}\right), \\ \mathbf{u} \times \boldsymbol{\omega} &= (u\zeta - v\eta, v\xi - w\zeta, w\eta - u\xi) \\ \text{and} \quad \mathbf{u} \times 2\boldsymbol{\Omega} &= 2\Omega(v\sin\theta, v\cos\theta, -w\sin\theta - u\cos\theta). \end{aligned} \tag{A 5}$$

Suppose we have evaluated $v_{j,k-1}, v_{j+1,k}$, etc., at $t^{n+\frac{1}{2}}$. Then the rotation term $\oint (\mathbf{u} \times 2\boldsymbol{\Omega}).d\mathbf{l}$ can be evaluated without interpolation along the contour C_{jk}, but because of the staggered mesh $\xi = (rs)^{-1}\partial(vs)/\partial\theta$ and $\eta = r^{-1}\partial(vr)/\partial r$ will not be available at the required points for use in the advection terms and will have to be obtained by interpolation. The relevant terms represent only curvature

effects (their sum vanishes in the Cartesian limit $r, s \to 1$) and are generally small, so that it is better to interpolate there than in the more important rotation terms. Therefore, in the following, we take

$$\xi_{jk} = (2r_j s_k \delta)^{-1} \Delta_\theta(sd), \quad \eta_{jk} = (2r_j h)^{-1} \Delta_r(rd), \tag{A 6}$$

where $d_{jk} = \frac{1}{4}(v_{j+1,k} + v_{j-1,k} + v_{j,k+1} + v_{j,k-1})$. Evaluating the required contour integrals and dividing by the relevant areas, we find

$$\begin{aligned}(\zeta_{jk}^{n+1} - \zeta_{jk}^n)/\Delta t = {} & (4r_j h\delta)^{-1}\{2h(g_j' T_{j,k-1}) - 2h(g_j' T_{j,k+1})\}^{n+\frac{1}{2}} \\ & + 2\Omega(4r_j h\delta)^{-1}\{(v_{j,k-1}s_{k-1})(2h) + (2r_{j+1}\delta)(v_{j+1,k}c_k) \\ & - (v_{j,k+1}s_{k+1})(2h) - (2r_{j-1}\delta)(v_{j-1,k}c_k)\}^{n+\frac{1}{2}} \\ & + \nu(r_j h\delta)^{-1}\{(hr_j^{-1}\delta^{-1})[s_{k+\frac{1}{2}}^{-1}(\zeta_{j,k+1}s_{k+1} - \bar{\zeta}_{jk}s_k) \\ & + s_{k-\frac{1}{2}}^{-1}(\zeta_{j,k-1}s_{k-1} - \bar{\zeta}_{jk}s_k)] \\ & + (\delta/h)[(\zeta_{j+1,k}r_{j+1} - \bar{\zeta}_{jk}r_j) + (\zeta_{j-1,k}r_{j-1} - \bar{\zeta}_{jk}r_j)]\}^{n+\frac{1}{2}} \\ & + (4r_j h\delta)^{-1}\{2h(u\zeta - v\eta)_{j,k-1} - 2h(u\zeta - v\eta)_{j,k+1} \\ & + (2r_{j+1}\delta)(v\xi - w\zeta)_{j+1,k} - (2r_{j-1}\delta)(v\xi - w\zeta)_{j-1,k}\}^{n+\frac{1}{2}}, \end{aligned} \tag{A 7}$$

where $g_j' = \alpha g(r_j)$. It proved more convenient to do the computations in terms of $Q = \zeta rs$ and so the equation actually used is obtained by multiplying (A 7) by $r_j s_k$ and regrouping the terms in $\bar{\zeta}_{jk}$ to obtain an explicit formula for Q_{jk}^{n+1}.

To find ψ_{jk} from Q_{jk}, we expand ψ in a double Taylor series about (r_j, θ_k), and arrange values from neighbouring points to obtain an approximation to (17). One such formula is

$$\begin{aligned} -Q_{jk} = {} & (2r_j^2\delta^2)^{-1}\{\psi_{j-1,k-1} + \psi_{j+1,k-1} + \psi_{j+1,k+1} + \psi_{j+1,k-1} \\ & + \tfrac{1}{2}(\psi_{j-2,k} + \psi_{j+2,k}) - 3\psi_{jk}\} + (4h^2)^{-1}\{\psi_{j-2,k} + \psi_{j+2,k} - \psi_{jk}\} \\ & + (\cot\theta_k/4r_j^2\delta)\{\psi_{j-1,k-1} + \psi_{j+1,k-1} - \psi_{j-1,k+1} - \psi_{j+1,k+1}\} \\ & + O(h^2) + O(\delta^2), \end{aligned} \tag{A 8}$$

in which it is clear how the various derivatives are represented. This formula is used except for $j = 2$ (near the centre) and $j = J - 1$ (near the surface), where it breaks down, but an alternative formula applies:

$$\begin{aligned} -Q_{jk} = {} & (\cot\theta_k/4r_j^2\delta)\{\psi_{j-1,k-1} + \psi_{j+1,k-1} - \psi_{j-1,k+1} - \psi_{j+1,k+1}\} \\ & + (2h^2)^{-1}\{\psi_{j-1,k-1} + \psi_{j-1,k+1} + \psi_{j+1,k-1} + \psi_{j+1,k+1} \\ & - \tfrac{1}{2}(\psi_{j,k+2} + \psi_{j,k-2}) - 3\psi_{jk}\} \\ & + (4r_j^2\delta^2)^{-1}\{\psi_{j,k+2} + \psi_{j,k-2} - 2\psi_{jk}\} + O(h^2) + O(\delta^2). \end{aligned} \tag{A 9}$$

Either (A 8) or (A 9) is solved for ψ_{jk} by successive relaxation (Smith 1965, p. 148). At each time step the iterations are deemed to have converged when

$$\max|\psi_{jk}^{(n)} - \psi_{jk}^{(n-1)}|/\max|\psi_{jk}| < \epsilon, \tag{A 10}$$

where $\psi_{jk}^{(n)}$ is the value of ψ_{jk} after n iterations at that time step, and $\epsilon \sim 10^{-3}$, a suitably small number. Convergence usually took only two or three iterations; using over-relaxation factors $\chi > 1$ yielded little improvement.

Unfortunately, to advance (T, v, ζ) at the next half time step requires ψ at precisely those points where we have not yet found it. But, remembering that Q satisfies (17), we find by manipulation of the Taylor series that

$$\begin{aligned}\psi_{jk}(2h^{-2}+2r^{-2}\delta^{-2}) &= h^{-2}(\psi_{j-1,k}+\psi_{j+1,k})+r^{-2}\delta^{-2}(1+\tfrac{1}{2}\delta\cot\theta_k)\psi_{j,k-1}+r^{-2}\delta^{-2}(1-\tfrac{1}{2}\delta\cot\theta_k)\psi_{j,k+1}\\ &\quad -\tfrac{1}{4}(Q_{j,k+1}+Q_{j,k-1}+Q_{j+1,k}+Q_{j-1,k})+O(h^4)+O(\delta^4), \qquad \text{(A 11)}\end{aligned}$$

from which the missing values can be found to adequate accuracy (cf. Moore *et al.* 1973).

The formula (A 1) breaks down at the axis ($j = 1$ or $k = 1$ or $k = L$) as various elements of area degenerate into lines, but by integrating (2) over appropriately shaped elements of volume surrounding the axis, we can retain a conservative scheme for T. One such elementary volume is the sphere V_c of radius h surrounding the origin (or a slice $\Delta\phi$ thereof). We define T_c to be the average temperature in this volume, and take all references by (A 1) to $T_{1,k}$ to refer to T_c. Then the increase of heat in V_c in the time interval (t^n, t^{n+1}) may be written as

$$(T_c^{n+1}-T_c^n)V_c = \sum_k{}' A_k + \sum_k{}' D_k + HV_c\Delta t, \qquad \text{(A 12)}$$

where A_k and D_k represent the fluxes of heat by advection and diffusion respectively through the face $r = r_2$, $\theta_{k-1} \leqslant \theta \leqslant \theta_{k+1}$ and the sum takes due account of the staggered mesh and the peculiarities at $k = 1$ and $k = L$ (where the face is only 'half-size'). The diffusion term is actually estimated from the flux through the face $r = \frac{1}{2}h$, so that (A 12) becomes eventually

$$\begin{aligned}T_c^{n+1}(1+c_1\Sigma' s_k) &= T_c^n(1-c_1\Sigma' s_k)+2c_1\Sigma' s_k T_{2,k}\\ &\quad +H\Delta t+(\tfrac{3}{2}h^{-3}\Delta t)\,\Sigma' T_{2,k}(\psi_{2,k+1}-\psi_{2,k-1}), \qquad \text{(A 13)}\end{aligned}$$

where

$$c_1 = 12(\kappa\Delta t)\,h^{-4}r_{\frac{3}{2}}^2\sigma.$$

Owing to an algebraic error, almost all the calculations used half this value of c_1, so that T_c as calculated is about $\frac{1}{2}\%$ too high when $J = 16$. The overall effect of this discrepancy has been verified to be negligible.

Similarly, when $k = 1$ (the northern axis), we take $T_{j,1}$ to be the average temperature over the 'frustrum' V_1 bounded by the axis, the face $\theta = \theta_2\,(= \delta)$, and the faces $r = r_{j\pm1}$. The diffusion terms are evaluated over the small box V_1' bounded by $\theta = \frac{1}{2}\delta$, $r = r_{j\pm\frac{1}{2}}$; the other terms are integrated over V_1 to yield

$$\begin{aligned}(T_{j,1}^{n+1}-T_{j,1}^n)V_1 &= HV_1\Delta t+T_{j,2}(\psi_{j+1,2}-\psi_{j-1,2})\,\Delta t\\ &\quad -T_{j+1,1}(\psi_{j+1,2}-\psi_{j+1,1})\,\Delta t+T_{j-1,1}(\psi_{j-1,2}-\psi_{j-1,1})\,\Delta t\\ &\quad +\kappa\Delta t(V_1/V_1')\{s_{\frac{3}{2}}r_j h\delta^{-1}(T_{j,2}-\overline{T}_{j,1})\\ &\quad +(2\sin^2(\tfrac{1}{4}\delta)/h)\,[r_{j+\frac{1}{2}}^2(T_{j+1,1}-\overline{T}_{j,1})+r_{j-\frac{1}{2}}^2(T_{j-1,1}-\overline{T}_{j,1})]\}. \qquad \text{(A 14)}\end{aligned}$$

A similar formula holds when $k = L$.

The other axis conditions (21) are trivial to implement, as are the surface conditions (18). To implement the flux boundary conditions (20), we use the standard method of 'dummy points' at $r_{J+1} = 1+h$ (Smith 1965, p. 32) and set

$$v_{J+1\,k}/r_{J+1} = v_{J-1,k}/r_{J-1} \tag{A 15}$$

and (remembering that $\psi_{J,k} = 0$)

$$\psi_{J+1,k}/r^2_{J+\frac{1}{2}} = -\psi_{J-1,k}/r^2_{J-\frac{1}{2}}. \tag{A 16}$$

Then ζ can be evaluated at the surface by (19) as

$$\zeta_{J,k} = -(\psi_{J+1,k}+\psi_{J-1,k})/h^2. \tag{A 17}$$

REFERENCES

Baldwin, P. 1967 *Proc. Camb. Phil. Soc.* **63**, 855.

Batchelor, G. K. 1956 *J. Fluid Mech.* **1**, 177.

Batchelor, G. K. 1967 *An Introduction to Fluid Dynamics*. Cambridge University Press.

Bisshopp, F. E. 1958 *Phil. Mag.* **3**, 1342.

Bodenheimer, P. 1971 *Astrophys. J.* **167**, 153.

Brebbia, C. A. & Connor, J. J. (eds) 1974 *Numerical Methods in Fluid Dynamics*. London: Pentech Press.

Busse, F. H. 1970*a* *J. Fluid Mech.* **44**, 441.

Busse, F. H. 1970*b* *Astrophys. J.* **159**, 629.

Busse, F. H. 1973 *Astron. Astrophys.* **28**, 27.

Chandrasekhar, S. 1961 *Hydrodynamics and Hydromagnetic Stability*. Oxford: Clarendon Press.

Durney, B. 1970 *Astrophys. J.* **161**, 1115.

Foster, T. D. 1969 *J. Fluid Mech.* **37**, 81.

Fricke, K. J. & Kippenhahn, R. 1972 *Ann. Rev. Astron. Astrophys.* **10**, 45.

Gough, D. O. & Lynden-Bell, D. 1968 *J. Fluid Mech.* **32**, 437.

Graham, E. 1975 *J. Fluid Mech.* **70**, 689.

Hsui, A. T., Turcotte, D. L. & Torrance, K. E. 1972 *Geophys. Fluid Dyn.* **3**, 35.

Krishnamurti, R. 1970 *J. Fluid Mech.* **42**, 295.

Moore, D. R., Peckover, R. S. & Weiss, N. O. 1973 *Comp. Phys. Comm.* **6**, 198.

Moore, D. R. & Weiss, N. O. 1973 *J. Fluid Mech.* **58**, 289.

Morton, K. W. 1971 *Proc. Roy. Soc.* A **323**, 237.

Orszag, S. A. & Israeli, M. 1974 *Ann. Rev. Fluid Mech.* **6**, 281.

Parker, E. N. 1963 *Astrophys. J.* **138**, 226.

Peckover, R. S. & Weiss, N. O. 1972 *Comp. Phys. Comm.* **4**, 339.

Roberts, K. V. & Weiss, N. O. 1966 *Math. Comp.* **20**, 272.

Roberts, P. H. 1968 *Phil. Trans. Roy. Soc.* A **263**, 93.

Rossby, H. T. 1969 *J. Fluid Mech.* **36**, 309.

Schwarzschild, M. 1958 *Structure and Evolution of the Stars*. Princeton University Press.

Segel, L. A. 1966 In *Non-equilibrium Thermodynamics, Variational Techniques, and Stability* (ed. R. J. Donnelly, R. Herman & I. Prigogine), p. 165. Chicago University Press.

Simon, G. W. & Weiss, N. O. 1968 *Z. Astrophys.* **69**, 435.

Smith, G. D. 1965 *Numerical Solution of Partial Differential Equations*. Oxford University Press.

Somerville, R. C. J. & Lipps, F. B. 1973 *J. Atmos. Sci.* **30**, 590.

TAYLER, R. J. 1973 *Mon. Not. Roy. Astr. Soc.* **165**, 39.
VERONIS, G. 1959 *J. Fluid Mech.* **5**, 401.
VERONIS, G. 1966*a* *J. Fluid Mech.* **26**, 49.
VERONIS, G. 1966*b* *J. Fluid Mech.* **24**, 545.
VERONIS, G. 1968 *J. Fluid Mech.* **31**, 113.
WEIR, A. D. 1975 *Mém. Soc. Roy. Sci. Liège*, Sér. 6, **6**, 37.
WEISS, N. O. 1964 *Phil. Trans.* A **256**, 99.
WEISS, N. O. 1966 *Proc. Roy. Soc.* A **293**, 310.
YOUNG, R. E. 1974 *J. Fluid Mech.* **63**, 695.